

# Level 3 Algorithm Description

V01

AKATSUKI LEVEL 3 TEAM

## Update Log

Version	Date	Author	Diff
V00	2018-08-24	Ogohara, Murakami	
V01	2019-05-21	Murakami	Add description for treatment of isolated missing value or dead pixel value

## 1. Geometry of mapping

We introduce an instrument BASE coordinate as shown in Fig. 1. The X and Y axes in Fig. 1 represent those of the VCO\_IR1\_BASE, VCO\_IR2\_BASE, VCO\_LIR\_BASE or VCO\_UVI\_BASE coordinates described in the instrument and frame kernels. Points O, Q, C, P and P' mean the focal point of a camera, the location of the optical axis on the detector plane, the center of Venus, a certain point on the Venusian cloud layer and a point on which P is projected. The length of OQ,  $L_F$ , is the focal length of the camera. We assume that  $\overrightarrow{PO}$  is identical to  $\overrightarrow{PS}$  shown in Fig 2, which is a vector from  $P(\lambda, \varphi)$  to the spacecraft in the IAU\_VENUS frame.  $\overrightarrow{PO}$  in Fig. 1 is a product of  $\overrightarrow{PS}$  in Fig. 2 and a rotation matrix from the IAU\_VENUS frame to the frame VCO\_\*\_BASE, retrieved from the SPICE toolkit (<http://naif.jpl.nasa.gov/naif/toolkit.html>) and kernels. If we assume the pinhole-like model as the optical system of a camera as shown in Fig. 1, P' is derived from  $\overrightarrow{PO}$ . Therefore, once  $P(\lambda, \varphi)$  is specified, P' is also determined on the detector plane. Brightness at  $P(\lambda, \varphi)$  in longitude–latitude coordinate is determined by a simple bilinear interpolation of values on the nearest and the adjacent three pixels around P'. If one of more pixels to be used for bilinear interpolation have missing value or dead pixel value, pixel value at  $P(\lambda, \varphi)$  will be set to missing value. As for LIR image, if only one of the pixel has missing value or dead pixel value, the pixel value at  $(i, j)$  is replaced by average of adjacent four pixels, *i.e.*, pixels at  $(i-1, j)$ ,  $(i+1, j)$ ,  $(i, j-1)$ , and  $(i, j+1)$ , and then bilinear interpolation is calculated, where  $i$  and  $j$  are indexes of pixel in Level 2 data or Level 3x data.

## 2. Pointing correction by the limb-fitting technique

We let  $\overrightarrow{L_V}$  a unit vector from the focal point, O, to the center of Venus, C.  $\overrightarrow{L_V}$  in an instrument BASE coordinate system is shown in Fig. 3. Here although we can easily calculate  $\overrightarrow{L_V}$  in an instrument BASE frame using the SPICE toolkit, we have to redetermine  $\overrightarrow{L_V}$  based on the position and shape of a Venus disk because uncertainties of the alignment of the instrument and the attitude of the spacecraft are not negligible.  $\overrightarrow{L_V}$  derived from the SPICE kernels ( $\overrightarrow{L_{Vobs}}$  hereafter) disagrees with  $\overrightarrow{L_V}$  determined from based on the position and shape of a Venus disk ( $\overrightarrow{L_{Vfit}}$  hereafter). Venus is imaged as an ellipse (Fig. 3) because the boresight vector of a camera does not pass through the center of Venus in general. We assume the center and the semi-major axis of the ellipse  $D(x_c, y_c)$  and  $a$ , respectively. Using the azimuthal angle,  $\alpha$ , and the elevation angle,  $\beta$ , of  $\overrightarrow{L_V}$ , we can express  $\overrightarrow{L_{Vfit}}$  as:

$$\overrightarrow{L_{Vfit}} = \begin{pmatrix} \cos \beta \cos \alpha \\ \cos \beta \sin \alpha \\ \sin \beta \end{pmatrix} \quad (1)$$

$\alpha$  and  $\beta$  are expressed as:

$$\alpha = \arctan\left(\frac{y_c}{x_c}\right) + \pi, \quad (2)$$

$$\beta = \frac{\pi}{2} - \frac{1}{2} \left\{ \arctan\left(\frac{l-a}{L_F}\right) + \arctan\left(\frac{l+a}{L_F}\right) \right\}, \quad (3)$$

where  $l$  equals to  $\overline{QD}$  (Ogohara et al., 2012). If  $x_c$ ,  $y_c$  and  $a$  are determined from a Venus disk on an image, we can obtain  $\overline{L_{\text{Vfit}}}$  by substituting Eqs. (2) and (3) into Eq. (1). We can also calculate a rotation matrix  $R$  which rotates  $\overline{L_{\text{Vobs}}}$  about  $\overline{L_{\text{Vobs}}} \times \overline{L_{\text{Vfit}}}$  to obtain  $\overline{L_{\text{Vfit}}}$ . We obtain  $P'$  corrected based on the instrument pointing estimated from an image if we use  $\overline{PO}$  multiplied by  $R$  instead of  $\overline{PO}$ . The rotation angle,  $\gamma$ , is expressed as  $\cos^{-1}(\overline{L_{\text{Vobs}}} \cdot \overline{L_{\text{Vfit}}})$  (referred to as  $D\_LVANG$  in L3 and L3x data files).

$x_c$ ,  $y_c$  and  $a$  required for calculating  $\overline{L_{\text{Vfit}}}$  are determined by fitting an ellipse to the Venus limb. The position of the limb of a Venus disk (hereafter, limb point) has to be determined as accurately as possible. We let  $f = f(x_i)$ , ( $i = 1, 2, \dots, N$ ) a one dimensional distribution of radiance intersecting a limb in the direction of  $X_{\text{base}}$  at  $y = y_j$  ( $j = 1, 2, \dots, N$ ) on a certain image and assume that the absolute value of  $df(x)/dx$  reaches a maximum at  $x = x_{\text{imax}}$ . Using the nonlinear least square method, we fit the continuous function  $h$  given in the following equation to brightness data  $f(x_{\text{imax}-M})$ ,  $f(x_{\text{imax}-M+1})$ , ...,  $f(x_{\text{imax}+M})$ , on  $M$  points,  $(x_{\text{imax}-M}, y_j)$ ,  $(x_{\text{imax}-M+1}, y_j)$ , ...,  $(x_{\text{imax}+M}, y_j)$ :

$$h(x) = p \tanh\{q(x - r)\} + s \quad (4)$$

where  $p$ ,  $q$ ,  $r$  and  $s$  are fitting parameters. A pixel means an integrated value of a physical quantity over the pixel (Sakurai and Shin, 2001). So, the objective function,  $G$ , to be minimized is based on that used by Ogohara et al. (2012), except for the number of pixels used for the one-dimensional fitting.  $M$  is determined so that the variation of radiance from the space toward the Venus disk is included in the one-dimensional distribution of radiance. The value of  $r$  included in the set of best-fit parameters values ( $p$ ,  $q$ ,  $r$ ,  $s$ ) that minimize  $G$  is defined as the position of a limb point at  $y = y_j$ . In the case where the above one dimensional fitting is performed only in the direction of  $X_{\text{base}}$ , we cannot determine the limb points accurately around the regions where the limb is nearly parallel to the  $X_{\text{base}}$  axis because of the small gradient of the brightness in this direction. For these regions, the limb points are determined by fitting the same function to brightness distributions along the  $Y_{\text{base}}$  axis. Letting the sub spacecraft position in the instrument BASE coordinate and the Venus apparent radius ( $x_{\text{sscb}}$ ,  $y_{\text{sscb}}$ ) and  $R_{\text{ap}}$ , respectively, a limb point is searched in the  $X_{\text{base}}$

direction along the  $j$ -th row if  $|j - y_{\text{sscb}}| < R_{\text{ap}} \sin 45^\circ$ . If  $|i - x_{\text{sscb}}| < R_{\text{ap}} \sin 45^\circ$ , a limb point is detected by the  $Y_{\text{base}}$  direction search along the  $i$ -th column.

After the positions of limb points are determined, the six coefficients of the following ellipse equation are determined by fitting an ellipse to the limb points based on Ogohara et al. (2012):

$$Ax^2 + 2Bxy + Cy^2 + 2f_0(Dx + Ey) + f_0^2F = 0. \quad (5)$$

$f_0$  is a constant of order of  $x$  and  $y$  introduced to the equation for equalizing the dimension of the terms and keeping the precision of the calculation (Iwamoto et al., 2009). The extended FNS (EFNS) method for constrained parameter estimation (Kanatani and Sugaya, 2007a) is used for the ellipse fitting based on Kanatani and Sugaya (2007b). The initial guess for the EFNS method is prepared by the FNS method (Chojnacki et al., 2000; Kanatani and Sugaya, 2007b) and the initial guess for the FNS method is estimated by the HLS method (Iwamoto et al., 2009) instead of Taubin method (Taubin 1991), which is used by Ogohara et al. (2012). Once the six coefficients are determined by the ellipse fitting, we can calculate the semi-minor axis,  $b$ , and the argument of the semi-major axis,  $\theta$ , in addition to  $(x_c, y_c)$  and  $a$  defined in the above as follow:

$$\begin{pmatrix} x_c \\ y_c \end{pmatrix} = \frac{f_0}{AC - B^2} \begin{pmatrix} BE & CD \\ BD & AE \end{pmatrix}, \quad (6)$$

$$\tan 2\theta = \frac{2B}{A - C}, \quad (7)$$

$$a^2 = \frac{2}{a \left\{ (A + C) - \sqrt{(A - C)^2 + 4B^2} \right\}}, \quad (8)$$

$$b^2 = \frac{2}{a \left\{ (A + C) + \sqrt{(A - C)^2 + 4B^2} \right\}}. \quad (9)$$

### 3. Accuracy of pointing correction

The accuracy of pointing correction has been statistically estimated by Ogohara et al. (2017). The result showed that the algorithm we developed and used for Level-3 data worked well; the uncertainties in the sub-spacecraft point were about  $O(10^{-2} \sim 10^{-1})$  pixels. It is expected that the Level-3 data will be useful for deriving the CMVs accurately, except for some of the nightside images. It is noted, however, that the error estimation of the pointing correction was based on assumed ideal conditions. Therefore, we must pay attention to various factors such as the thermal conditions of the satellite and/or the uncertainty in the assumed cloud altitudes, which could affect the pointing correction. It has been reported by Ogohara et al. (2017), for example, that, in the nightside cases, the actual error of the pointing correction can become  $O(1)$  pixels, which is much greater than the  $O(10^{-1})$ -pixel

error they showed in Table 5. Actually, a westward jump of cloud features was seen over the whole domain and corresponded to about a  $30\text{-m}\cdot\text{s}^{-1}$  increase in the easterly wind speed in 2 hours. This jump is obviously unrealistic. Ogohara et al. (2017) reported that jumps larger than  $\sim 20\text{ m}\cdot\text{s}^{-1}$  were found in about one-third of all IR2  $2.26\text{ }\mu\text{m}$  cases where cloud tracking was successfully performed during the period from 2016-07-11 to 2016-09-06. L3-product users have to estimate the mapping accuracy for their particular topics (e.g., cloud tracking) by themselves if they use nightside images.

#### 4. Precaution for use

- Artificial jaggy features are often seen near areas with large emission angles in L3 brightness temperature data for LIR, which result from low spatial resolution. Hence, users have to trim the area in advance based on their research interests.

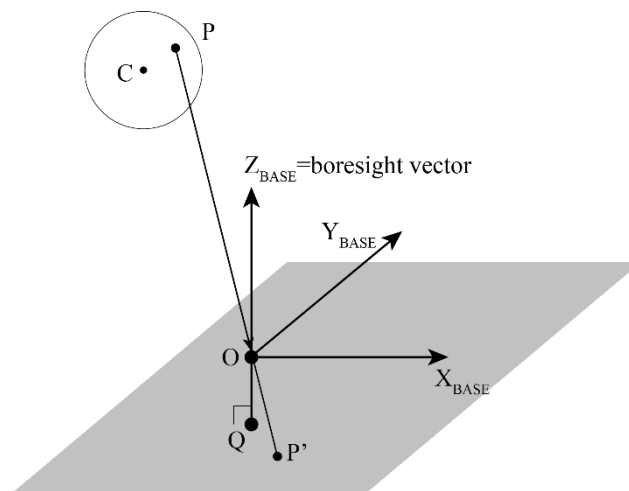


Figure 1 Schematic view of an instrument BASE coordinate and the position of Venus in the BASE coordinate. O is the focal point. Q is the intersection point between the boresight vector and the detector plane of the instrument. C and P are the Venus center and an arbitrary point on the surface of a sphere whose radius is the summation of the Venus radius and the assumed cloud altitude, respectively. P' is a point on the detector plane, on which P is projected if the optical system is assumed to be simplified as the pin-hole-like model.

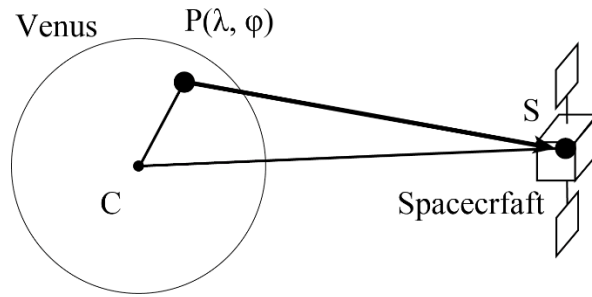


Figure 2 Schematic view displaying the positional relationship among the center of Venus, C, the position of the spacecraft, S, and a point at  $(\lambda, \varphi)$  on a sphere whose radius is the summation of the Venus radius and the assumed cloud altitude.

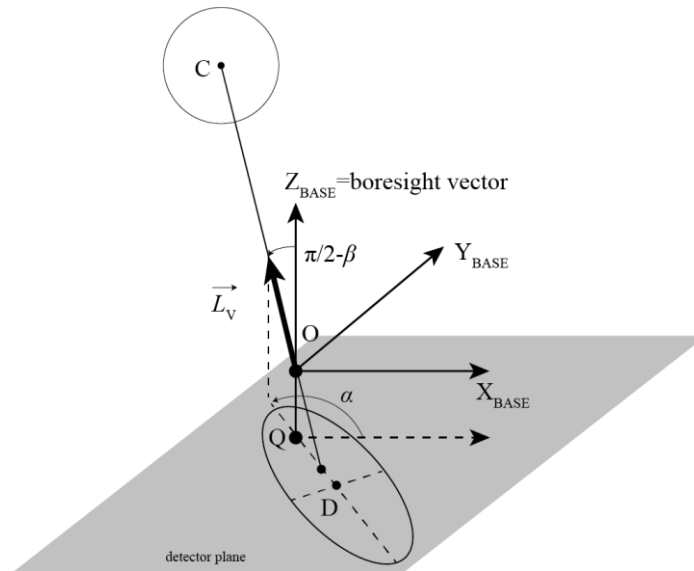


Figure 3 Schematic view of  $\vec{L}_V$  in the instrument BASE coordinate. An ellipse on the detector plane indicates the elliptic Venus disk. D is the center of the ellipse.

## References

Chojnacki, W., M. J. Brooks, A. van den Hengel and D. Gawley (2000), On the fitting of surfaces to data with covariances, IEEE Trans. Patt. Anal. Mach. Intell., 22, 11, 1294–1303. DOI:

[10.1109/34.888714](https://doi.org/10.1109/34.888714)

Iwamoto, Y., P. Rangarajan, and K. Kanatani (2009), Ellipse Fitting by Hyperaccurate Least Squares, IPSJ SIG Technical report. <http://id.nii.ac.jp/1001/00062747/>

Kanatani, K., and Y. Sugaya (2007a), Extended FNS for Constrained Parameter Estimation, in 10th Meeting on Image Recognition and Understanding, pp. 219–224, Hiroshima.

Kanatani, K., and Y. Sugaya (2007b), Performance evaluation of iterative geometric fitting algorithms, *Comput. Stat. Data Anal.*, 52(2), 1208–1222, DOI: [10.1016/j.csda.2007.05.013](https://doi.org/10.1016/j.csda.2007.05.013).

Ogohara, K., et al. (2012), Automated cloud tracking system for the Akatsuki Venus Climate Orbiter data. *Icarus* 217: 661–668, DOI: [10.1016/j.icarus.2011.05.017](https://doi.org/10.1016/j.icarus.2011.05.017).

Ogohara, K., et al. (2017), Overview of Akatsuki data products: definition of data levels, method and accuracy of geometric correction, *Earth, Planets and Space*, 69, 167, DOI: [10.1186/s40623-017-0749-](https://doi.org/10.1186/s40623-017-0749-5)